Portable Ultrasound System for Blood Velocity Estimation
Project Report

Master Thesis
April, 2023

Author:
Jeppe Hinrichs

Advisor(s):
Hyunjoo Lee, Xenofon Fafoutis, Tiberiu Gabriel Zsurzsan

Approval

This thesis has been prepared over six months at the Brain/Biomedical Microsystems Laboratory, School of Electrical Engineering, at the Korean Advanced Institute of Science and Technology, KAIST, and the Department of Electrical Engineering, Technical University of Denmark, DTU. This thesis is in partial fulfilment for the joint-degree Master of Science in Electrical Engineering, MSEE from KAIST and DTU.

Jeppe Hinrichs - s163555

.....

Signature

.....

Date

Contents

List of Figures

List of Tables

Abbreviations

Notation	Description
ADC	analogue-to-digital converter
BP	band-pass
CMUT	capacitive micromachined ultrasound transducer
CPU	central processing unit
CT	computed tomography
CW	continuous-wave
DSP	digital signal processor
DTU	Danmarks Tekniske Universitet (Technical University of Denmark)
I/O	input/output
IC	integrated circuit
KAIST	Korea Advanced Institute of Science and Technology
low-res	low resolution
MCU	microcontroller unit
MRI	magnetic resonance imaging
PSD	power spectral density
PW	pulsed-wave
RTOS	real-time operating system
US	ultrasound

Glossary

Notation	Description
adiabatic	Any process that happens without heat gain or loss is considered adiabatic
Doppler effect	A change in frequency of a wave in relation to an observer who is moving relative to the wave source
transcutaneous	Applied across the depth of the skin without invasive penetration

Nomenclature

Name	Unit	Description
		Input filter
V_{ref}	V	Reference voltage
C_{hp}	F	High pass filter capacitor
R_{hp}	Ω	High pass filter resistor
f_{hp}	Hz	High pass cut-off frequency
C_{lp}	F	Low pass filter capacitor
R_{lp}	Ω	Low pass filter resistor
f_{lp}	Hz	Low pass cut-off frequency
A_v	1	Amplification factor
		Modulator
R_1	Ω	AIM voltage divider resistor
R_2	Ω	AIM voltage divider resistor
R_{in}	Ω	AIM input resistor
R_{fb}	Ω	AIM feedback resistor
C_1	F	AIM capacitor
V_{in}	V	Input signal voltage
V_{span}	V	Voltage range of input signal
V_{pwm}	V	PWM signal
V_H	V	V_{pwm} high level voltage
V_L	V	V_{pwm} low level voltage
V_{out}	V	V_{pwm} voltage range ($V_H - V_L$)
V_{hys}	V	Hysteresis voltage
V_{hw}	V	Hysteresis width
V_{th_H}	V	Hysteresis threshold upper voltage
V_{th_L}	V	Hysteresis threshold lower voltage
V_c	V	PWM carrier voltage
V_{c_H}	V	PWM carrier upper voltage
V_{c_L}	V	PWM carrier lower voltage
f_{sw}	Hz	PWM signal frequency
D	1	PWM signal duty cycle
t_H	s	PWM carrier charge time

Continued on next page

Name	Unit	Description
t_L	s	PWM carrier discharge time
τ	1	PWM carrier charge constant
R_{th}	Ω	PWM carrier thevenin resistance
f_{idle}	Hz	PWM signal idle switching frequency
k_2	1	R_{fb}, R_{in} voltage divider
		Gate driver
D_{dt}	1	Dead-time circuit diode
R_{dt}	Ω	Dead-time circuit resistor
C_{dt}	F	Dead-time circuit capacitor
V_C	V	Dead-time circuit supply voltage
V_s	V	IC supply voltage
t_c	s	Charging circuit time
		Power stage
V_{DD}	V	Power supply voltage
Q_1, Q_2, Q_3, Q_4	1	Power stage switches
V_g	V	Gate driver signal
V_o	V	Output voltage
I_o	A	Output current
R_{BTL}	Ω	Speaker equivalent load resistance
		Output filter
R_f	Ω	Output filter single-ended load
C_{BTL}	F	Output filter differential capacitance
C_f	F	Output filter single-ended capacitance
L_f	H	Output filter inductance
ΔI_L	A	Output filter ripple current
Q	1	Output filter quality factor
f_c	Hz	Output filter cut-off frequency
ω_n	rads^{-1}	Output filter natural frequency
ζ	1	Output filter damping ratio

Continued on next page

Name	Unit	Description
		Shunt regulator
R_{sh}	Ω	Shunt current limiting resistor
I_K	A	Shunt cathode current
$I_{K_{\max}}$	A	Shunt maximum cathode current
$I_{K_{\min}}$	A	Shunt minimum cathode current
I_{su}	A	Shunt supply current
R_{A1}	Ω	Shunt adjust resistor 1
R_{A2}	Ω	Shunt adjust resistor 2
C_L	F	Shunt load capacitance
$V_{\text{ref}_{\text{IC}}}$	V	Shunt internal reference voltage

Reading comprehension

This section of the report will explain to the reader how to reference this document and explain the fundamental structure of the project as well as the report. Throughout the report, the reader will be assumed to be knowledgeable of basic circuit analysis and familiar with standard abbreviations typically used in electrical engineering. If not, readers can refer to the denotation section at the beginning of the report. It is assumed that the reader has a basic knowledge on the science of electrical engineering, physics, and circuit analysis.

Sources

Calculus expressions present in the report will typically have a reference explaining their origin. All references are prominently displayed with square brackets and a number, directing to the appendix in the last section of the report.

1 Introduction

The progress of diagnostic imaging has advanced significantly during the 20th century. As the cost of high-speed computational systems has grown increasingly accessible, so has the use of medical imaging become prominent. Potentially millions of people have been spared painful exploratory surgery through non-invasive diagnostic imaging. And thus, lives can be saved by early diagnosis and intervention through medical imaging. Advancements in scientific visualisation have in turn generated more complex datasets of increased size and quality. The four major technologies used are ultrasound (US), X-ray, computed tomography (CT), and magnetic resonance imaging (MRI). Each technology has distinct advantages and disadvantages in biomedical imaging, and thus each is still relevant for modern medicine. Table 1.1 contains a comparison and summary of the various fundamental diagnostic imaging modalities.

Since 2004, medical imaging has been reported to have been performed more than 5 billion times [8], and later numbers from 2011 show a general doubling and in particular, a tenfold increase in ultrasound examinations between 2000 and 2011 [20]. Recent data reveal that this trend of doubling has continued throughout the years 2010 to 2020 [32], and reveal that even though patient processes were disrupted during the global SARS-CoV-2 pandemic, the number of medical imaging examinations per 1000 patients still increased. The reasons for this and, particularly, why ultrasound has seen a significant increase in use, can be attributed to its high, but inconsistent, resolution, cost-effectiveness, portability, and real-time interventional imaging. The downside of ultrasound is its limited penetration and restrictions for use in certain body parts. When comparing soft tissue examinations, which ultrasound is limited to, both CT and MRI can image the entire body with consistent resolution and contrast, but are more expensive and have poor portability due to the immense size of their hardware.

The cardiovascular system, which transports oxygen and nutrients to tissue, produces a complex flow pattern that causes velocity fluctuations. Several cardiovascular diseases are also known to cause abnormal blood flow. As mentioned above, ultrasound is a powerful tool for performing non-invasive imaging of the cardiovascular system [16], [19], and has no adverse risk to patients. Determining power spectral density (PSD) of a received signal is a common way to estimate blood velocity. A processed image of PSD over time is commonly known as a sonogram, where changes in blood velocity over time can be seen.

1.1 Project scope

The aim of this project is to study the application of ultrasound in the context of blood flow measurements. Various scientific articles have been studied to gain knowledge of previous research [4]–[6], [9], [11], [13]–[15], [17], [18], [24], [25], [27]–[30]. In addition, textbooks [19]–[21] have also been instrumental in forming a solid knowledge base for the thesis. The desire is to build upon the vast knowledge already gathered by prominent researchers in the field of ultrasound systems for blood velocity estimation. Finally, using the knowledge gained, we designed and implemented an electronic device capable of performing these measurements using a novel approach. The system used in this project is called an Ultrasound Doppler flow-meter. Ultrasound Doppler flow-meters can be used to measure the velocity of blood flow in the human body. This is commonly done to assess the health of blood vessels and to diagnose and monitor conditions such as arteriosclerosis (hardening

Table 1.1: Comparison of medical imaging modalities

Modality	**Ultrasound**	**X-ray**	**CT**	**MRI**
Topic	Longitudinal, shear, mechanical properties	Mean X-ray tissue absorption	Local tissue X-ray absorbtion	Biochemistry (*T1* and *T2*)
Access	Small windows adequate	2 sides needed	Circumferential around body	Circumferential around body
Spatial resolution	0.2 mm to 3 mm[a]	$\sim$ 1 mm	$\sim$ 1 mm	$\sim$ 1 mm
Penetration	3 cm to 25 cm[b]	Excellent	Excellent	Excellent
Safety	Excellent	Ionizing radiation	Ionizing radiation	Very good
Speed	Real-time	Minutes	20 minutes	Varies[†]
Cost	$	$	$$	$$$
Portability	Excellent	Good	Poor	Poor
Volume coverage	Real-time 3D volumes, improving	2D	Large 3D volume	Large 3D volume
Contrast	Increasing (shear)	Limited	Limited	Slightly flexible
Intervention	Real-time 3D increasing	No[c]	No	Yes, limited
Functional	Functional ultrasound	No	No	fMRI

[a] Frequency and axially dependent.
[b] Frequency dependent.
[c] Fluoroscopy limited.
[†] Typical: 45 minutes, fastest: Real-time (*low-res*).

of the arteries) and deep vein thrombosis (blood clots in the veins). To measure blood velocity with an ultrasound Doppler flow-meter, a handheld probe is placed on the skin over the area of interest, such as an artery or vein. The probe contains a transducer that emits high-frequency ultrasound waves and receives the reflected waves. The Doppler shift in the frequency of the reflected waves is caused by the movement of the blood cells, and it is proportional to the velocity of the blood flow. The probe is connected to a portable ultrasound machine, which processes the Doppler shift and displays the velocity of the blood flow on a screen. The machine can also produce a color-coded map of the blood flow, which allows the user to visualize the velocity of the blood at different points within the vessel. Ultrasound Doppler flow-meters are non-invasive and safe to use, and they provide a quick and easy way to measure blood velocity. However, they are not always accurate, especially in cases where there is a high degree of turbulence or when there are air bubbles or solid particles present in the blood. They are also limited in their ability to

measure blood flow in small vessels or in deep tissues. The goals of the project are written in table 1.2.

Table 1.2: Project specification

Project specification
Study and research ultrasound and its principles and applications
Design and implement a device for ultrasound blood velocity estimation
Investigate and test the device in an experimental setting
Validate results with commercial equipment
Make quantifiable performance measurements on system
Write a technical report documenting the project work

The project is conducted under the guidance of advisors from the affiliated institutions Danmarks Tekniske Universitet (Technical University of Denmark) (*DTU*), Department of Electrical Engineering, Department of Applied Mathematics and Computer Science, and Korea Advanced Institute of Science and Technology (*KAIST*) at the Brain/BioMedical Microsystems Laboratory. The report is divided into five chapters, and the first part is an introduction to the project. The second chapter will focus on explaining the theory of the topic of the project. The third chapter focuses on the synthesis of a system for experimental testing. The fourth chapter explains the production of the hardware. The fifth chapter will explain the testing methodology performed on the hardware. Finally, additional documentation of testing, code, circuit diagrams, and laboratory setups can be found in the appendix.

2 Theory

This chapter explains the overall theory that forms the fundamental principles of this project. Initially, the characteristics of ultrasound will be explained from an acoustics standpoint. Then, a brief overview of the systemic circulation is explained in vivo. Lastly, the various types of flow-meters are outlined with their strengths and weaknesses.

2.1 Ultrasound

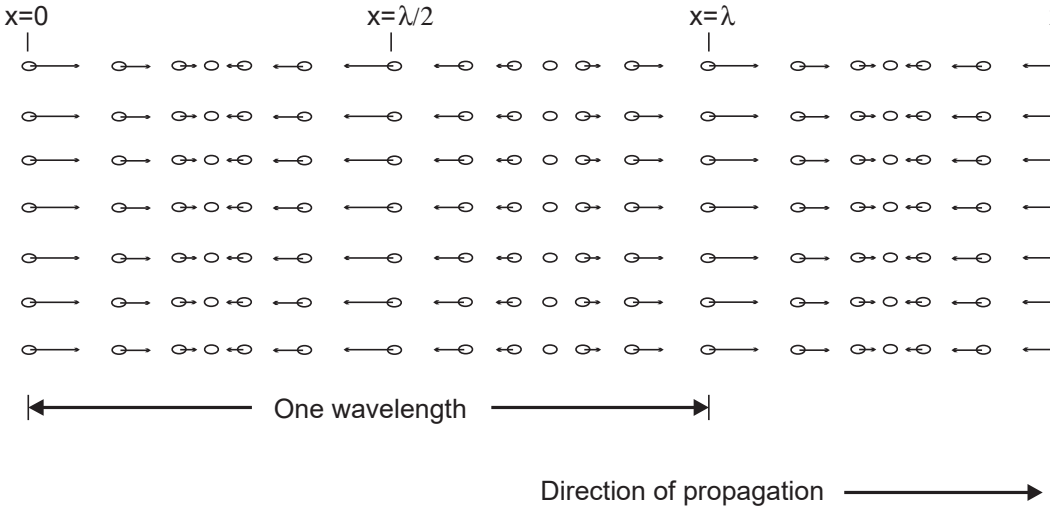

Figure 2.1: Particle displacement for a propagating ultrasound wave [19]

US is a technology that transmit sound wave with frequencies above the audible range (20 to 20 000 Hz) to mechanically vibrate matter. The particles in the medium would be at rest and distributed uniformly before any disturbance. The wave propagates as a disturbance and the particles oscillate around their mean position due to the presence of the ultrasonic wave. Typically the *US* frequency band used in clinical settings are from 1 to 15 MHz [20]. Figure 2.1 visualizes the propagation of a plane wave in matter. The oscillation occurs parallel to the wave's direction, making it longitudinal, and the disturbance will propagate with the variable c, which is determined by the medium and is given by eq. (2.1).

$$c = \sqrt{\frac{1}{\rho_0 \kappa_S}} \tag{2.1}$$

Where ρ_0 is the mean density (kgm^{-3}) and κ_S is the adiabatic compressibility ($\mathrm{m}^2\mathrm{N}^{-1}$). Since in the majority of cases, the propagation of ultrasound is linear, it is assumed in this work. The acoustic pressure of the harmonic plane wave is expressed by eq. (2.2).

$$p(t, z) = p_0 e^{j(\omega t - kz)} \tag{2.2}$$

And propagates along the z-axis. ω is the angular frequency, k is the wave number and is expressed by $k = \omega/c = 2\pi/\lambda$, and $_0$ is the acoustic pressure amplitude. A spherical wave is expressed by eq. (2.3)

$$p(t, r) = p_0 e^{j(\omega t - kr)} \tag{2.3}$$

Where r is radial distance, and is defined in a polar coordinate system. For each time instance, the acoustic pressure $p(t, r)$ is constant over a fixed radial position. In this scenario, the pressure amplitude is given by $p_0(r) = {}^{k_p}/_{r}$, where k_p is a constant since the energy of the outgoing wave must be constant. Particle speed u is dependent on the pressure caused by a wave expressed by eq. (2.4)

$$u = \frac{p}{Z} \tag{2.4}$$

Where Z is the characteristic acoustic impedance, defined as the ratio of acoustic pressure to particle speed at a given position in the medium and is expressed by eq. (2.5).

$$Z = \rho_0 c \tag{2.5}$$

Characteristic acoustic impedance Z is one of the most significant variables in the characterization of propagating plane waves. Reference values for density, speed of sound, and characteristic acoustic impedance can be seen in table 2.1.

Table 2.1: Approximate density, sound speed, and acoustic impedance of human tissue types [19]

Medium	**Density** (ρ_0) kg/m^3	**Speed of sound** (c) m/s	**Acoustic impedance** (Z) kg/(m^{2}s)
Air	1.2	333	0.4×10^3
Blood	1.06×10^3	1566	1.66×10^6
Bone	$1.38–1.81 \times 10^3$	2070–5350	$3.75–7.38 \times 10^6$
Brain	1.03×10^3	1505–1612	$1.55–1.66 \times 10^6$
Fat	0.92×10^3	1446	1.33×10^6
Kidney	1.04×10^3	1567	1.62×10^6
Lung	0.4×10^3	650	0.26×10^6
Liver	1.06×10^3	1566	1.66×10^6
Muscle	1.07×10^3	1542–1626	$1.65–1.74 \times 10^6$
Spleen	1.06×10^3	1566	1.66×10^6
DI	1×10^3	1480	1.48×10^6

In the following sections, various acoustic wave phenomena will be briefly described.

2.1.1 Scattering

A wave propagating through a medium continues in the same direction until it encounters a new medium. When this occurs, a portion of the wave is transmitted into the new medium with a change in direction. Because the scattered wave is the result of several contributors, it is necessary to define it statistically. The amplitude distribution is Gaussian [19] and can thus be fully described by its mean and variance. The mean value is zero because the dispersed signal is caused by variances in the acoustic characteristics in the tissue. The correlation between multiple data is what allows ultrasound to determine blood velocities. Because minor movements have a significant correlation, it is feasible to discover alterations in location by comparing sequential measurements of moving structures, such as blood cells. In medical ultrasound, only one transducer is used to transmit and receive, and only the backscattered signal is analysed. The power of the scattered signal is defined by the

scattering cross-section, which in small cases means a uniform intensity I_i, and is expressed by eq. (2.6).

$$P_s = I_i \sigma_{sc} \tag{2.6}$$

Where σ_{sc} is the scattering cross-section in square meters. The backscattering cross section is material dependant and determines the intensity of the scattering. If the dispersed energy is evenly emitted in all directions, the scattered intensity is given by eq. (2.7).

$$I_s = \frac{P_s}{4\pi R^2} = \frac{\sigma_{sc}}{4\pi R^2} \cdot I_i \tag{2.7}$$

Where R is distance to the scattering region [19]. This results in a spherical wave. A transducer with radius r gives the power P_r, presuming the attenuation and focus is neglected, and is expressed by eq. (2.8).

$$P_r = I_s \pi r^2 = \sigma_{sc} \frac{r^2}{4R^2} \cdot I_i \tag{2.8}$$

The backscattering coefficient, which characterizes scattering from a volume of scatterers, is another measure of scattering strength. It is defined as the average received power per steradian volume of scatterers when flooded with plane waves of unit amplitude and the unit is 1/cmsr. Backscattering coefficients in the blood are significantly lower than the backscattering coefficients from various tissue types. This poses a challenge when estimating blood flow close to tissue vessel walls [3], [19].

2.1.2 Attenuation

The ultrasonic wave will be reduced as it propagates through the tissue due to absorption and scattering. The attenuation in tissue is frequency dependent, with greater attenuation with increasing frequency. Because of absorption and dispersion, the ultrasonic wave will be attenuated as it travels through the tissue. The relationship between attenuation, distance travelled, and frequency is often linear. Attenuation in the tissue occurs as a result of both dispersion, which spreads energy in all directions, and absorption, which turns it into thermal energy.

Table 2.2: Approximate attenuation values for human tissue [19]

Tissue	**Attenuation** dB/(MHz · cm)
Liver	0.6–0.9
Kidney	0.8–1
Spleen	0.5–1
Fat	1–2
Blood	0.17–0.24
Plasma	0.01
Bone	16–23

The pressure of a wave propagating in z-direction decreases exponentially expressed by eq. (2.9)

$$p(z) = p(z = 0)e^{-\alpha z} \tag{2.9}$$

Where $p(z = 0)$ is the pressure in the point of origin and α is the attenuation coefficient. The attenuation coefficient unit is Npcm^{-1} and, alternatively, dBcm^{-1} with the relationship described in eq. (2.10).

$$\alpha = \frac{1}{z} \ln \frac{p(z = 0)}{p(z)} \tag{2.10a}$$

$$\alpha(\mathrm{dBcm}^{-1}) = 20(log_{10}e)\alpha(\mathrm{Npcm}^{-1}) = 8.68\alpha(\mathrm{Npcm}^{-1}) \tag{2.10b}$$

The significance of absorption and scattering in ultrasonic attenuation in biological tissues is a point of contention. Scattering adds just a few per cent to attenuation in most soft tissues. As a result, it is fair to conclude that absorption is the primary mechanism of ultrasonic attenuation in biological tissues [21].

2.1.3 Transducer

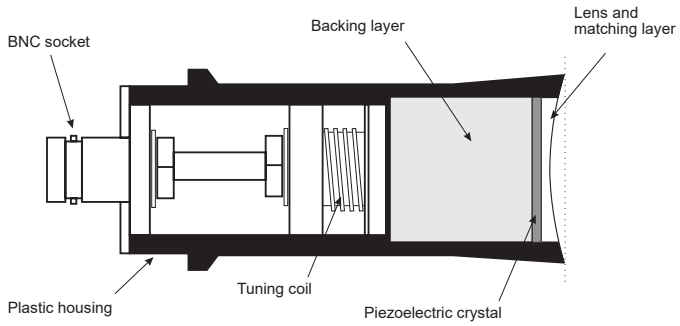

Figure 2.2: Single element ultrasound transducer construction [19]

A layperson knows transducers as speakers and microphones in the context of PA systems. In the case of medical *US* it is the device that generates the acoustic pressure field, which is emitted into the tissue. The transducer has a piezoelectric crystal inside the housing. When excited, this crystal emits ultrasound waves toward flowing blood. The red blood cells will reflect a fraction of the emitted waves. These reflected waves are of a different frequency than the transmitted wave. If the red blood cells move away from the transducer, the frequency will be lower. If the red blood cells are moving towards the transducer, the frequency will be higher. This is caused by the Doppler effect. The reflected ultrasonic waves return to the crystal and are converted back into electrical signals. The single-element transducer shown in fig. 2.2 has a minimal imaging window and has to be mechanically manipulated to obtain a wide window, which is unfeasible for responsive high-frequency imaging. Thus, usually, a transducer array is used. Various types of *US* transducer exist with different strengths and weaknesses, shown in fig. 2.3.

2.1.4 Doppler effect

The Doppler effect is a phenomenon in which an observer perceives a shift in the frequency of sound emitted from a source when either the source or the observer is moving, or both are moving. The reason for the perceived change in frequency is visualised in fig. 2.4. In diagram (a), the source S_p is stationary and produces a spherical distribution pattern of the wave with the perceived frequency of the observer is given by $f = {}^{c}/_{\lambda}$, where c is the velocity of the wave in the medium and λ is the wavelength. In diagram (b), the sound source is moving towards the right with a velocity v. The locomotion of the source changes the distribution pattern and causes a longer wavelength on the left, indicating a lower

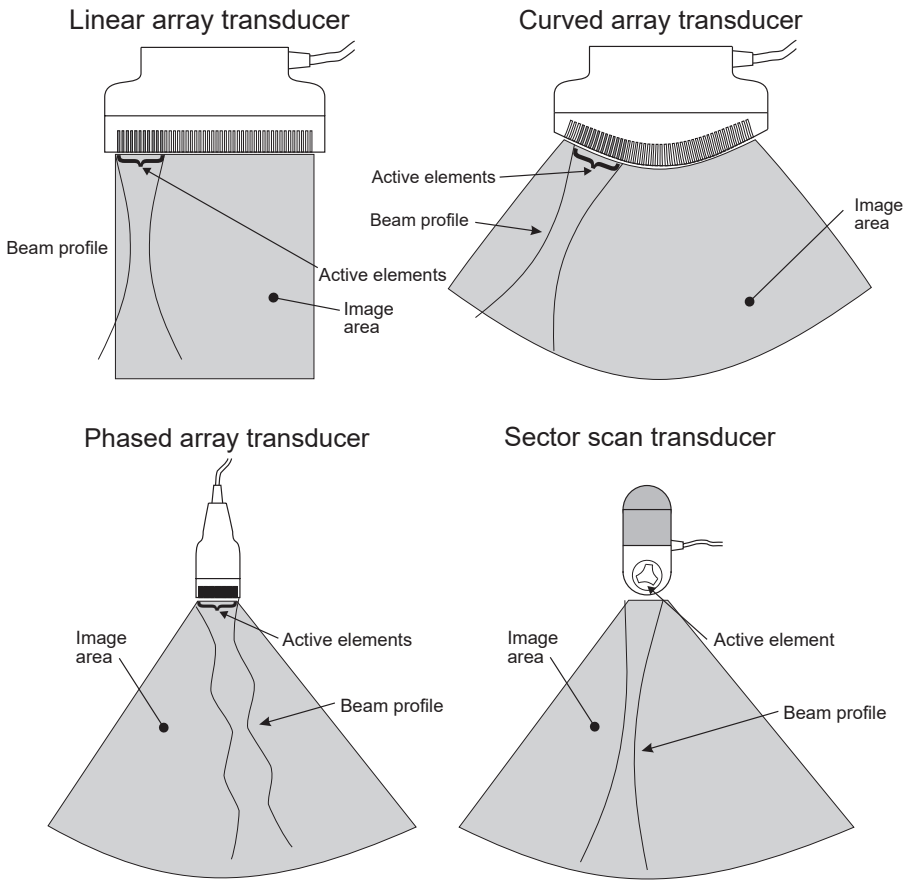

Figure 2.3: Transducer types for acquiring B-mode images [19]

perceived frequency, and a shorter wavelength on the right, indicating a higher perceived frequency, both denoted as λ' in the diagram. In the case of the observer on the right side, the perceived frequency becomes eq. (2.11).

$$f' = \frac{c}{\lambda} = \frac{c}{\lambda - vT} = \frac{c}{(c-v)T} = \frac{c}{c-v} \cdot f_0 \tag{2.11}$$

And viceversa, on the left side, the perceived frequency becomes eq. (2.12).

$$f' = \frac{c}{c+v} \cdot f_0 \tag{2.12}$$

Where Hvad mangl

This perceived difference between the frequency that is transmitted from the source f_0, and the perceived frequency f' is also called the Doppler frequency, f_d. When these connections are combined, the Doppler frequency for a source moving with velocity v and an observer travelling with velocity v' is given by eq. (2.13).

$$f_d = f' - f = \left(\frac{c+v'}{c-v} - 1\right) \tag{2.13}$$

If both source and observer are moving with the same velocity, v, assuming $c \gg v$, the v cancels out and the expression is reduced to eq. (2.14).

$$f_d = \frac{2vf}{c} \tag{2.14}$$

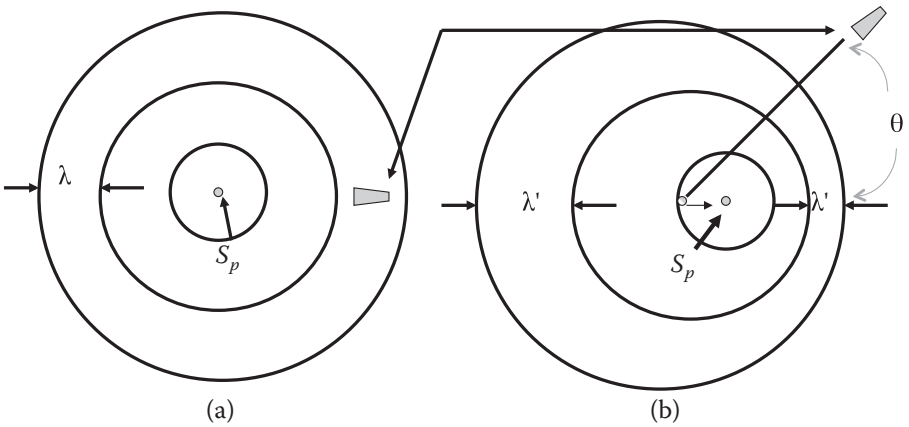

Figure 2.4: Doppler effect diagram. A stationary observer perceives a change in the frequency of a wave generated by a moving source toward the observer as a result of a wavelength shift from λ to λ'. In (a), the source is still. In (b), the source is moving at a velocity v. [21]

If the velocity of the moving source is traveling with an incident angle θ, the v in eq. (2.14) is replaced with $v(\cos\theta)$. This results in the expression found in eq. (2.15) and forms the basis for applied Doppler effect measurements.

$$f_d = \frac{2v(\cos\theta)f}{c} \tag{2.15}$$

The Doppler effect is used in ultrasonic Doppler devices used to image blood flow transcutaneously. An ultrasonic transducer in these devices sends ultrasonic waves into a blood artery, and the scattered radiation from moving red cells is measured by either the same transducer or a second transducer. The Doppler frequency, which is determined by the velocity of red blood cells, is extracted using modern electronic demodulation techniques.

2.2 Flow Physics

The flow physics of the human circulatory system are sophisticated, and numerous nonstationary flow patterns emerge. The human circulatory system takes care of transporting oxygen and nutrients to organs, as well as disposing of waste products produced by metabolism. It is possible because the blood within the circulatory system contains several smaller subcomponents, such as plasma and formed cellular elements that perform these vital functions. Initially, blood is discharged from the left ventricle of the heart through the aorta and travels to all areas of the body through multiple branches of the arterial tree. When blood flows through the arteries, it enters smaller channels known as arterioles. These arterioles lead to a network of tiny capillaries through which nutrients and waste materials are exchanged between the blood and the organs. The capillaries connect to form a network of venulae, which supply the veins and deliver blood back to the heart. This system, in its entirety, is called systemic circulation. A diagram of the circulatory system as described above can be seen in fig. 2.5. In summary, when examining the elements that comprise the circulatory system, it consists of several components:

- Heart, the primary organ of the circulatory system that maintains blood pressure and controls blood velocity.
- Blood, and its sub-components

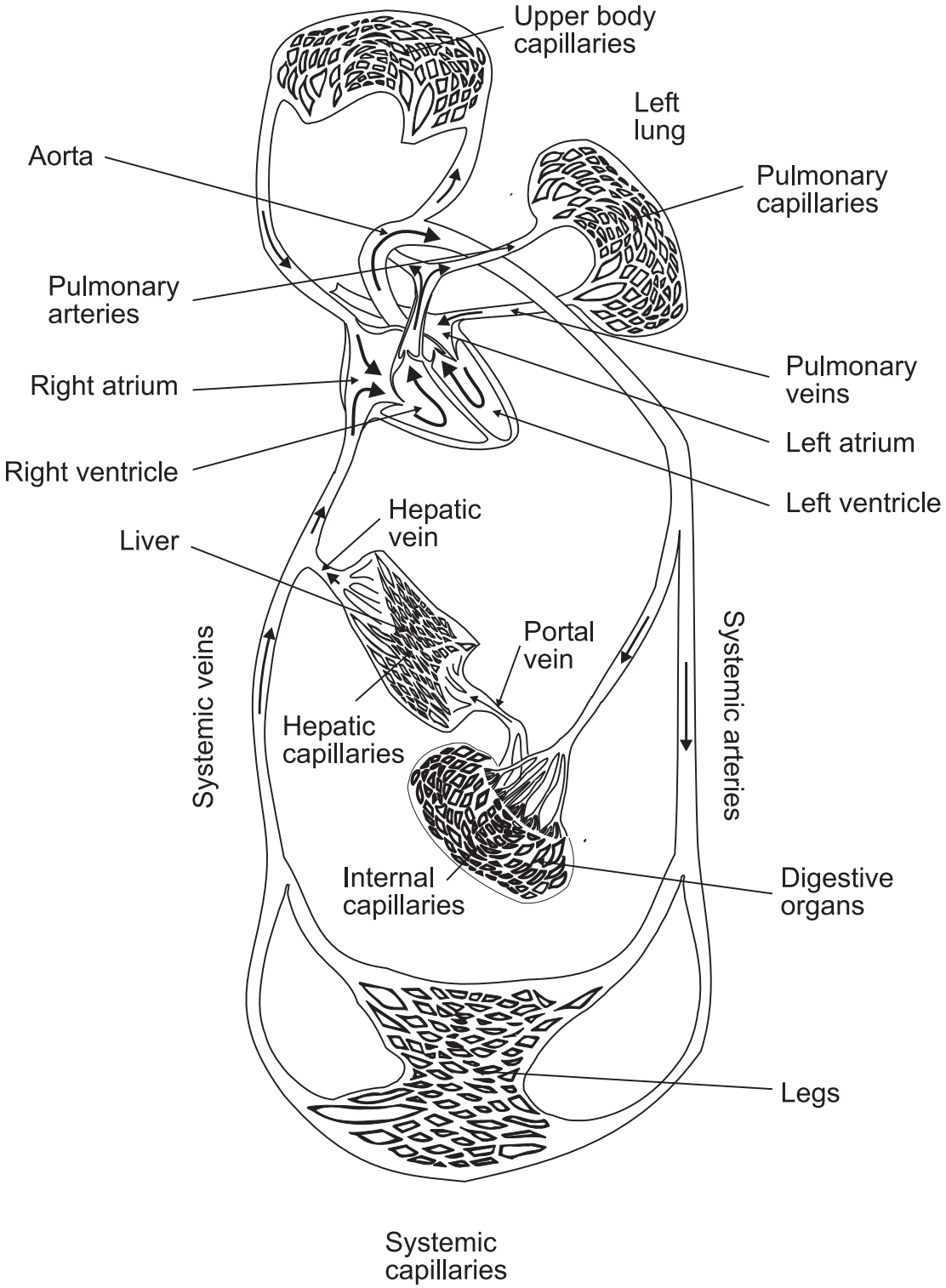

Figure 2.5: Circulatory system of the human body [19]

– Plasma, which forms the primary volume and contains nutrients and formed cellular elements.

– Red and white blood cells, which carry oxygen and fight off infections, respectively.

  - Platelets, which are also known as thrombocytes, have the function of clotting during blood vessel injury.

- Blood vessels
  - Arteries (and arterioles), transport oxygenised blood to organs and tissues at high pressure and velocity.
  - Capillaries are thin but wide-ranging blood vessels that perform the exchange of matter between the circulatory system and tissue.
  - Veins (and venules) carry blood back to the heart at low pressure and velocity.

2.2.1 Blood flow

Blood flow is the amount of blood that goes through a blood vessel in a particular period of time, and has a complicated flow pattern due to its pulsing flow. Advanced analysis of haemodynamics is not within the scope of this report, so the explanation will be brief. The primary forces that determine the blood flow F are the pressure difference across a blood vessel and vascular resistance. It is determined by Ohm's law as in eq. (2.16).

$$F = \frac{\Delta P}{R} \tag{2.16}$$

Where ΔP is the pressure difference across the blood vessel and R is the vascular resistance. The pressure difference ΔP is calculated with eq. (2.17).

$$\Delta P = P_1 - P_2 \tag{2.17}$$

Where P_1 and P_2 are the blood pressures measured at each end of the blood vessel. Pressure has a significant importance on blood flow because an increase in arterial pressure not only increases the force that pushes blood through the capillaries but also expands the vessels, lowering vascular resistance.

2.3 Devices

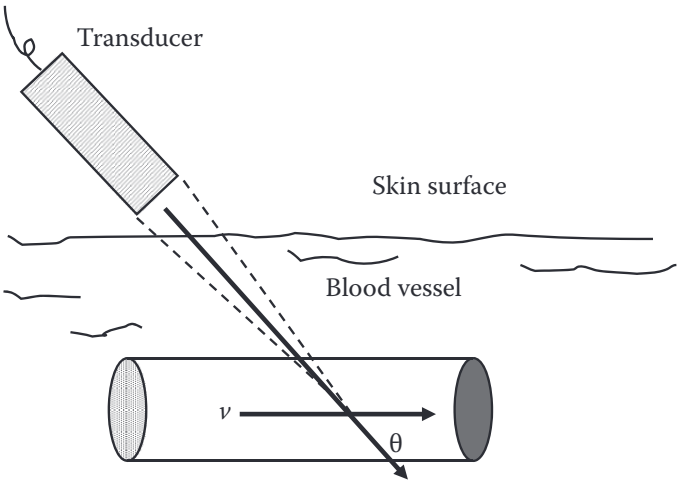

Figure 2.6: Diagram of *US* wave transmitted and reaching blood vessel with incident angle θ [21]

A device that measures the flowing of blood is called a flowmeter. Flowmeters may be used both inside and outside of vessels. One of the flowmeters that may be used outside

the vessel to monitor flow is US. Figure 2.6 depicts an ultrasonic wave of frequency f insonifying a blood artery, resulting in an angle of θ relative to velocity v. For simplicity, it is assumed that blood flows in a vessel at a constant velocity v. The echoes returned are shifted in frequency as described in eq. (2.15) earlier in the chapter. The echoes scattered by blood after being insonified by an ultrasonic wave convey information about the velocity of blood flow. Blood flow measurements are often used in clinical settings to determine the status of blood vessels and organ functioning. The two commonly used fundamental techniques for ultrasound Doppler flow measurements are continuous-wave (CW) and pulsed-wave (PW). Both will be explained.

2.3.1 Continuous-wave Flowmeter

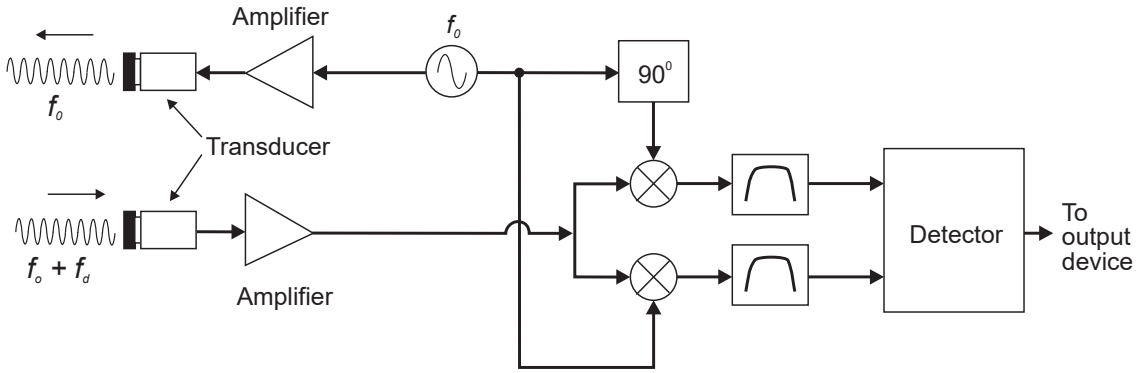

Figure 2.7: Block diagram of CW flowmeter [19]

The earliest non-invasive cardiovascular diagnostic technologies relied heavily on CW Doppler flowmeters. One of the earliest concepts for a device to estimate and study blood flow was proposed by Satomura, Yoshida, Mori, *et al.*[1] during the 1950s in Japan. To continuously transmit waves and receive signals from moving reflectors, the CW flowmeter uses two transducers. CW flowmeters use less sophisticated electronics than PW flowmeters. A drawback to the CW flowmeter is the lacking depth discrimination due to the continuous characteristic of this device type. A block diagram of a typical CW flowmeter can be seen in fig. 2.7. The basic principles of the device are previously explained in section 2.1.4, and the measurement of the device is described in eq. (2.11). The device continuously emits an ultrasonic wave in the first transducer expressed as a function of time by eq. (2.18) [19].

$$e(t) = \cos(2\pi f_0 t) \tag{2.18}$$

While receiving the backscattered signal on the second transducer expressed by eq. (2.19) [19].

$$r_s(t) = a\cos\left(2\pi f_0 \alpha(t - t_0)\right) \tag{2.19}$$

$$\alpha \approx 1 - \frac{2v_z}{c} \tag{2.20}$$

$$\alpha t_0 \approx \frac{2d_0}{c} \tag{2.21}$$

Where v_z indicates the velocity in the z direction. Applying the Fourier transform, the expression yields eq. (2.22).

$$r_s(t) \cdot e^{j2\pi f_0 t} \Longleftrightarrow R_s(f - f_0) \tag{2.22}$$

Where $R_s(f - f_0)$ is the Fourier transform of $r_s(t)$. The received signal is then multiplied with a quadrature signal of frequency f_0 to find the Doppler frequency in eq. (2.23).

$$m(t) = a\left[\cos(2\pi f_0 t) + j\sin(2\pi f_0 t)\right]\cos(2\pi f_0 \alpha(t - t_0)) \tag{2.23}$$

$$\begin{aligned} &= \frac{a}{2}\Big\{\cos(2\pi f_0[(1-\alpha)t - \alpha t_0]) + \cos(2\pi f_0[(1-\alpha)t - \alpha t_0]) \\ &\quad + j\sin(2\pi f_0[(1-\alpha)t - \alpha t_0]) + j\sin(2\pi f_0[(1-\alpha)t - \alpha t_0])\Big\} \end{aligned} \tag{2.24}$$

As is general for quadrature demodulation, the resulting signal contains the frequency components of the sum and difference of the emitted and received signals' frequencies shown in fig. 2.8, where the signals are shown in time and frequency domains.

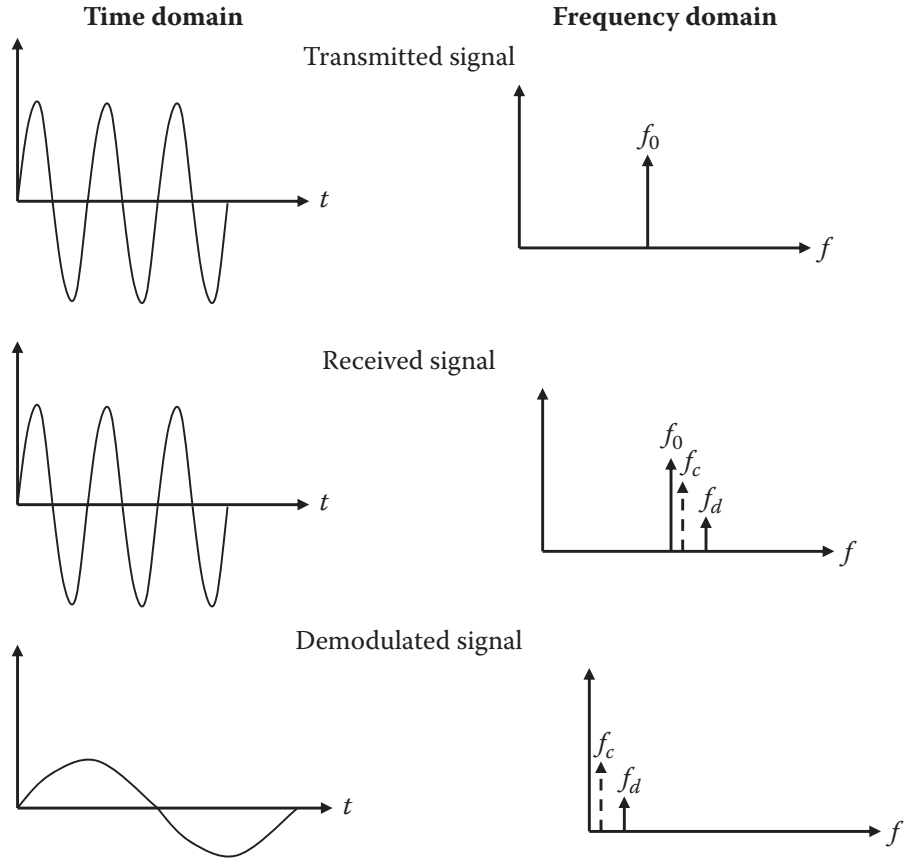

Figure 2.8: Doppler signals in time and frequency domain showing demodulation effects [21]

Generally, a band-pass (BP) filter is used on the demodulated signal to remove the high-frequency summed signal at twice the frequency of f_0. The filtered signal after the BP filter is expressed by eq. (2.25) and contains the Doppler shift of the emitted signal.

$$m_f(t) \approx \frac{a}{2} e^{\left(j2\pi f_0 \frac{2v_z}{c} t\right)} e^{(-j2\pi f_0 \alpha t_0)} \tag{2.25}$$

Where the second exponential term is the delay proportional to the time between transmission and receiving of the signal. The selected cutoff frequency is chosen to be much lower than the carrier frequency to remove the carrier wave. One issue with ultrasonic Doppler

blood flow monitoring is that the blood vessels that generate large reflected echoes are also moving with a low velocity. These big, slow-moving echoes are referred to as clutter signals in Doppler nomenclature. The band pass filter's low-end cutoff frequency must be designed to minimize interference from these clutter signals. The design of this band pass filter in the low-frequency region, which serves the function of high pass, also known as a clutter rejection filter, has proven troublesome since the magnitude of clutter signals is many orders greater than that of blood and may obfuscate those from slow-moving blood.

Table 2.3: Measured frequency shifts with a Doppler 3 MHz transducer at various velocities at a 45° incident angle [19]

Velocity (v) m/s	**Doppler frequency** (f_d) Hz
0.01	28
0.1	276
0.5	1377
1	2755
2	5510
5	13 770

Seen in table 2.3 is an example of measured Doppler frequencies using a 3 MHz transducer using the method shown in fig. 2.6. Note that the measured frequencies are all within the audible range.

2.3.2 Pulsed-wave Flowmeter

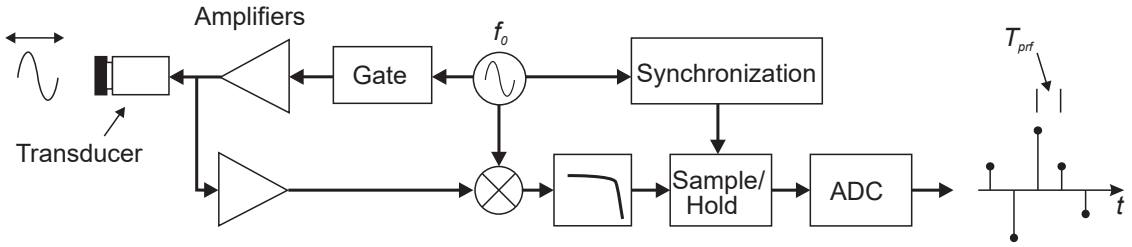

Figure 2.9: Block diagram of PW flowmeter [19]

The concept of a pulsed-wave flowmeter was proposed in [2] and other related articles. This type of flowmeter is periodically changing from a transmitter to a receiver. In the transmit mode, the transducer emits a series of pulses. When in the receiving mode, the transducer is listening for the backscattered signal. A simplified block diagram can be seen in fig. 2.9. The movement of particles within the blood causes a displacement in the backscattered signal. These systems are commonly referred to as "Doppler systems" even though it is somewhat misleading. The effects of attenuation are also causing a shift in frequency of a higher magnitude than the velocity of particles in the blood. This is because the conventional Doppler effect is not the straightforward methodology that is applied to the analysis of the back-scattered signal. It is, in fact, an artefact. It is the shift in the location of the scatters that is observed, not the shift in the transmitted frequency. Figure 2.10 shows the received signal after demodulation and filtering; the depth in tissue is fixed here, and the signals displayed on the left side of the figure are the result of a pulse sequence. Each line represents a single pulse, and each pulse is emitted at a pulse

repetition frequency, f_{prf}. Instead, on the right, the dotted line shows the sampled signal formed by taking into account the amplitude of each pulse after a specified time period.

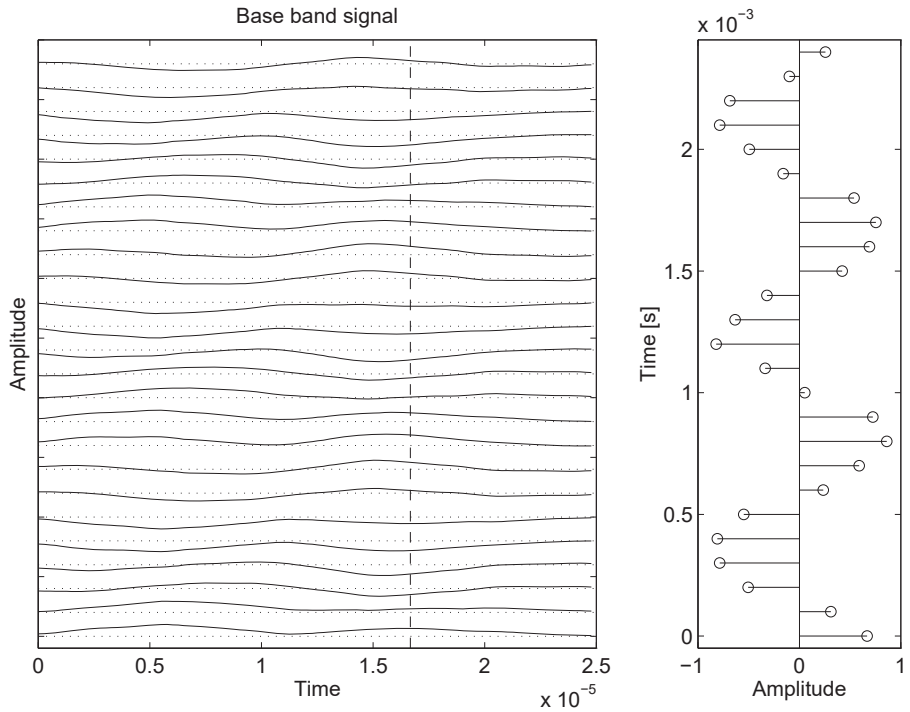

Figure 2.10: Sampling for a gate pulsed wave system with a single range. To depict the signals on the graph, a single pulse is emitted for each line, and the signals are displaced in amplitude. The sampled signal is displayed on the right. [19]

After the back-scattered signal is received it is multiplied by the centre frequency of the emitted pulse and filtered to remove the sum frequency [19]. A analogue-to-digital converter (ADC) quantifies the signal for further signal processing. Referring to displacement fig. 2.10 again, the dashed vertical line represents the sample of each pulse that is taken. If sampling is done T_s after pulse emission, the measurement depth is expressed by eq. (2.26).

$$d_0 = \frac{T_s c}{2} \tag{2.26}$$

Hypothetically, if the velocity of stationary scatterers in blood was measured, a constant amplitude would be measured. A change in the sample value is observed when there is movement. Between two pulses, the scatterer movement is proportional to the velocity v_z in the direction of the ultrasound beam. The time shift of t_s is expressed as eq. (2.27).

$$t_s = \frac{2v_z}{c} \cdot T_{\text{prf}} \tag{2.27}$$

Where c is the speed of sound, and T_{prf} is the timespan between each pulse emission. Taking one sample from each line at a certain depth yields a sampled signal with a frequency proportional to the scatter velocity. Thus, if a sample is taken at the same depth for each line, resulting in a sinusoidal signal proportional in frequency to the scatter velocity [7] and that signal is expressed by eqs. (2.28a) and (2.28b).

$$r(i) = a(i) \sin\left(2\pi f_p T_{\text{prf}} \cdot i\right) \tag{2.28a}$$

$$f_p = \frac{2v_z}{c} f_0 \tag{2.28b}$$

Where $a(i)$ is the amplitude, f_0 is the emitted frequency, and θ is the phase factor in the depth of interest. This technique improved the accuracy of the investigations of blood vessels and facilitated the display of velocity profiles. Furthermore, by employing two transducers or a multi-element transducer, duplex mode imaging (displaying both a B-mode picture and a blood velocity estimate) became feasible. Two-transducer systems are no longer utilised since it is easier to create a duplex picture with a multi-element transducer.

Hvor er θ i udtrykket? Omskriv fra Jensen2012

2.4 Blood Velocity Estimation

Once a backscattered signal is received, estimation of velocity can be obtained with multiple methods. In this section the most common methods to estimate blood velocity are mentioned with their strengths and limitations.

2.4.1 Spectral estimation

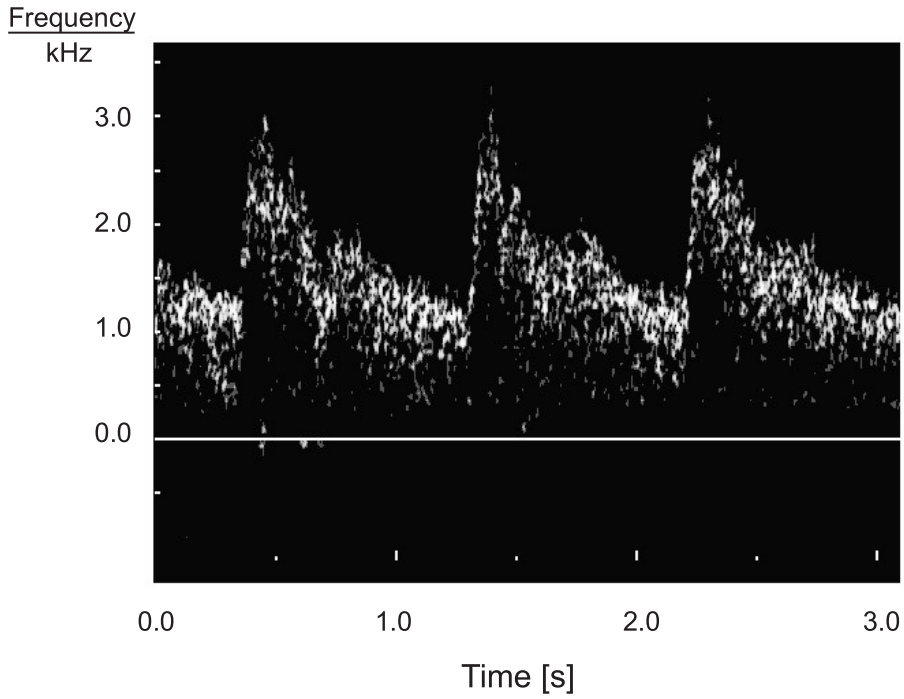

Figure 2.11: Arterial sonogram with time-frequency and Doppler shift [19]

Given that the frequency volume of the received signal is similar to the blood's velocity distribution, the Fourier transform of the received signal can be used to obtain velocity. The spectrogram, usually erroneously known as the Doppler spectrum, can be created by saving the *PSD* together. The *PSD* is calculated for each of the components that make up the received signal in order to accomplish this. A quadrature demodulated signal is used to display both positive and negative frequencies. When these spectra are shown side by side, the evolution of the velocity distribution can then be seen. A sonography of an artery is displayed in fig. 2.11.

3 Synthesis

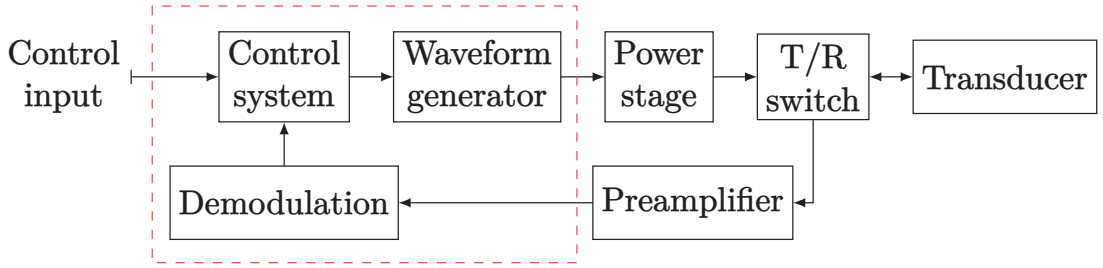

Figure 3.1: Simplified overview of the system with the demodulation and control system indicated with a red dashed rectangle

A simplified overview of the entire system can be seen in fig. 3.1. Each of the various modules will be explained during this chapter of the report. Initially, the control system will be briefly explained and the reasons for its design choice. Secondly, the signal chain in the transmitter will be outlined and how the transducer is driven by the power stage with the added protective switching circuit. Finally, the analogue front-end will be further explained with its various subcircuits for amplifying and demodulating the signal. Lastly, the design of the digital signal processor (DSP) within the control system will be explained.

3.1 Control System

The choice of platform for the control system is a microcontroller. A microcontroller is a small computer that is built into a single integrated circuit (IC) chip. It includes a central processing unit (CPU), memory, and input/output (I/O) peripherals, and it is designed to perform a specific set of tasks. Microcontrollers are used in a wide range of electronic devices, including appliances, automobiles, industrial control systems, and consumer electronics. Microcontrollers are often used in applications where a small, low-power device is needed to perform simple tasks, such as controlling a motor or reading a sensor. They are usually programmed in a high-level language, such as C or C++, and they can be programmed to perform a variety of tasks, depending on the specific application. The chosen microcontroller unit (MCU) for this project is STM32F411RE, because it is sufficient for the application and sourcing limitations within the IC supply chain. In addition, the selected development environment was Visual Studio Code with PlatformIO and Zephyr RTOS. Both are explained in the following subsections.

3.1.1 PlatformIO

PlatformIO is an open-source ecosystem for embedded development. It is designed to help developers build applications for various microcontrollers, such as Arduino, Raspberry Pi, and others. PlatformIO is available as a plugin for many popular integrated development environments (IDEs), including Visual Studio Code, Atom, and CLion. PlatformIO manages the project dependencies, builds and uploads code to microcontrollers, and debugs the applications. It also includes a library manager, which allows developers to easily include and manage external libraries and frameworks in their projects. PlatformIO is a cross-platform tool, which means it can be used on various operating systems, including Windows, macOS, and Linux. It is a popular choice for embedded development because of its ease of use and powerful features. PlatformIO works by downloading and setting

up a set of tools and libraries that allows building, uploading, and debugging various microcontrollers. It includes a library manager, a build system, and a debugger, as well as support for a wide range of microcontrollers and development boards. To use PlatformIO, it is installed as an extension to the preferred integrated development environment (IDE) Visual Studio Code. Then, a new PlatformIO project can then we created by select the desired microcontroller and development board, and specify any external libraries or frameworks they need to include. In this case, Zephyr RTOS is used as a framework. PlatformIO's build system takes care of compiling the code and linking it with any required libraries or frameworks. The debugger allows for stepping through the code and inspect variables, set breakpoints, and troubleshooting bugs.

3.1.2 Zephyr

Zephyr is an open-source real-time operating system (*RTOS*) designed for the Internet of Things (IoT). It is a lightweight RTOS that can run on a wide range of devices, from microcontrollers with as little as 20 KB of RAM to more powerful systems with multiple processors. Zephyr is designed to be modular and scalable, with a focus on security and low power consumption. It includes support for a wide range of hardware architectures, including ARM Cortex-M, x86, and RISC-V, and it can be used with a variety of development boards and microcontrollers. One of the key features of Zephyr is its ability to run on very small devices with limited resources. It includes support for various networking protocols, such as Bluetooth Low Energy (BLE), IPv4, and IPv6, which makes it well-suited for use in IoT applications. Zephyr is developed as part of the Linux Foundation's Zephyr Project, and it is widely used in the development of IoT and embedded systems. It is a popular choice for lightweight, flexible, and secure RTOS projects.

Real-Time Operating Systems

A real-time operating system is an operating system that is designed to handle real-time applications. Real-time applications are those that require timely processing of data in order to function correctly. This can include tasks such as controlling industrial machinery, monitoring and controlling processes. Real-time operating systems are designed to prioritize certain tasks and ensure that they are completed within a specific timeframe. They do this by allocating a certain amount of processing resources to each task, and by interrupting the execution of lower-priority tasks as needed to ensure that high-priority tasks are completed on time. RTOSs typically include features such as preemptive scheduling, real-time communication, and support for multiple processors and hardware architectures.

3.2 Pulse-Width-Modulation Generator

Initially, a waveform generator was designed by using a programmable synthesizer circuit, but due to constraints within generating dead-time when driving the half-bridge, a more accurate timer based PWM generation is required. In a half-bridge power stage, dead-time refers to the amount of time that elapses between the moment when one of the switches in the half-bridge (either the high-side or the low-side switch) turns off and the moment when the other switch turns on. During the dead-time, both switches in the half-bridge are off, which means that there is no current flowing through either switch in the half-bridge. A scenario where both switches are on, can cause problems if the output of the half-bridge is connected to a load, as it may cause the load to behave erratically or even be damaged. To avoid these problems, it is important to carefully consider the amount of dead-time in a half-bridge power stage. In general, a longer dead-time will reduce the risk of damage to the load, but it will also reduce the efficiency of the power stage, as energy will be lost

during the dead-time. Therefore, the designer must carefully balance the trade-off between efficiency and safety in order to determine the optimal amount of dead-time for a given half-bridge power stage. A complementary timer

3.3 Power Stage

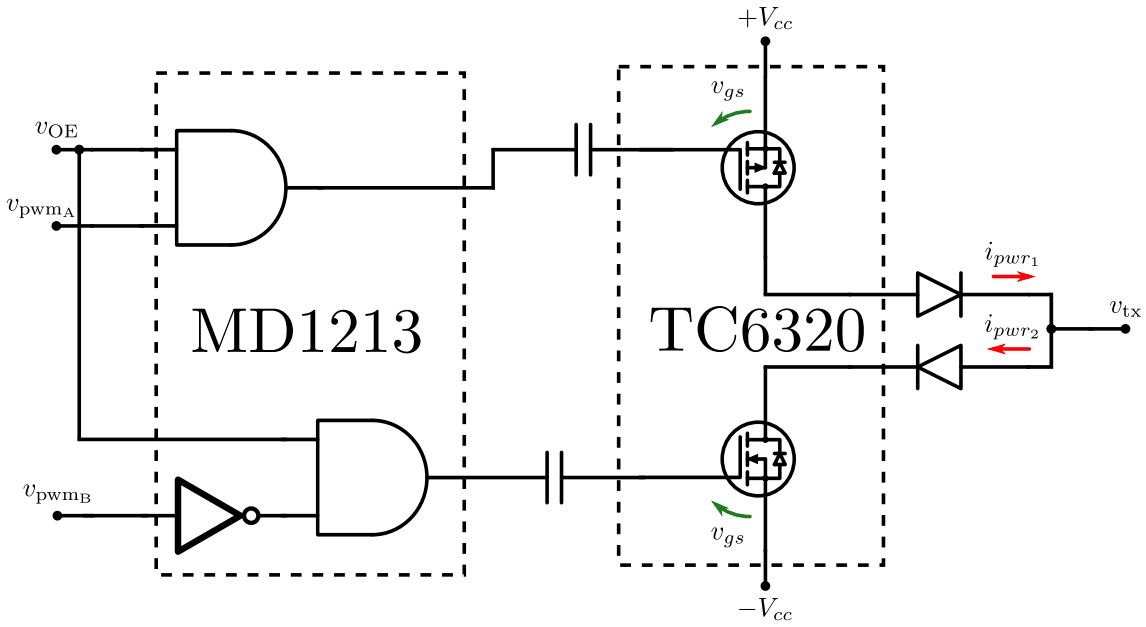

Figure 3.2: Circuit diagram of power stage

Gate drivers [10], [26], [31]

3.4 Transmit/Receive Switch

The transmit/receive switch is a module that is based on an IC from Texas Instruments known as TX810. The TX810 is an electronic device that can be used to switch transmit and receive paths of an ultrasound system. It can switch the transmit and receive paths for up to 8 different transducers (also known as probes) at the same time. The TX810 is programmed to switch the transmit and receive paths at specific times, as determined by the user. For example, the user can program the TX810 to switch the transmit and receive paths of a particular transducer at a specific time during the ultrasound examination. This allows the user to perform multi-channel imaging, where multiple transducers are used simultaneously to capture images from different angles. The IC is typically used in conjunction with an ultrasound system and one or more transducers. Transducers are used to transmit and receive ultrasound waves, which are used to generate images of the body's internal structures. The TX810 is used to switch the transmit and receive paths for each transducer at the appropriate times, allowing the ultrasound system to capture images from multiple angles simultaneously. When high-voltage transmitter signals are applied to the input, the internal diodes limit the output voltage. While in receive mode, the TX810's insertion loss is minimized. The TX810 features a 3-bit interface that may be used to program bias current from 7 mA to 0 mA for varying performance and power requirements, unlike conventional T/R switches. The device is put up in power-down mode when the TX810 bias current is set to 0mA (high-impedance mode). The TX810 does not put significant load on high-voltage transmitters when operating in the high-impedance

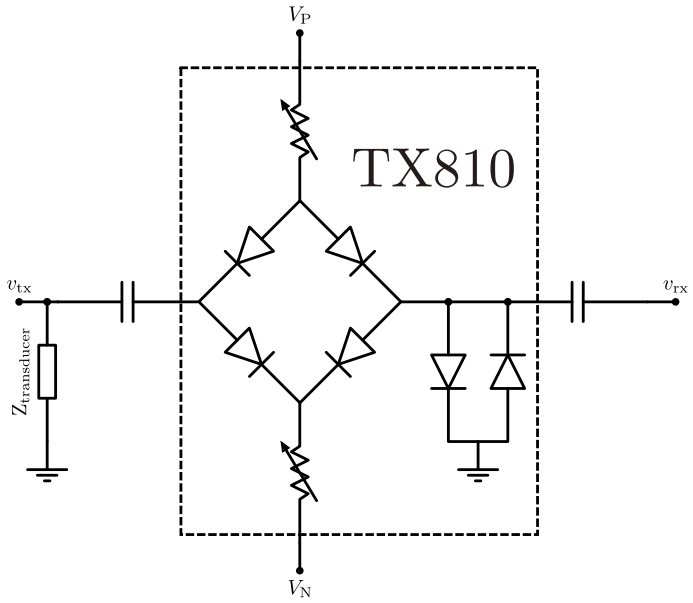

Figure 3.3: Circuit diagram of switch (per channel)

mode. The device can also wake up from power-down mode in less than a ţs. These sophisticated programmable features enable systems to save a large amount of electricity.

The module is designed with three channels available. That means three channels can be used, either three separate transducers for multi-angle sonography, or a capacitive micromachined ultrasound transducer ($CMUT$) with three channels in a single angle.

3.5 Transducer

3.5.1 Impedance matching input

3.6 Preamplifier

OPA487

The OPA847[12] is a high-performance, high-speed, voltage feedback amplifier with a bandwidth of over 1 GHz. It has a wide gain range, low distortion, and low noise, making it suitable for a variety of applications including video, RF, and high-speed data acquisition. The OPA847 has a single-ended input and a differential output, which allows it to be used in a variety of circuit configurations. It is available in a surface-mount package and operates over a wide supply voltage range.

AD8332

The AD8332[22] is a fully integrated, single-chip amplifier designed for use in a wide range of RF and microwave applications. It is a low-noise, high-linearity amplifier that can be used in a variety of configurations, including as a stand-alone amplifier or as part of a larger system. The AD8332 is a current-feedback amplifier that can operate over a wide frequency range, from 50 MHz to 4 GHz. It has a high level of integration, with all active components on a single monolithic IC. This makes it suitable for use in small form factor applications where space is at a premium. The AD8332 has a number of features that make it well-suited for use in RF and microwave applications. It has a high level of linearity, which allows it to amplify signals without introducing significant distortion. It also has a low noise figure, which makes it well-suited for use in low-noise applications. Additionally, the AD8332 has a wide dynamic range, which makes it capable of handling a wide range

of input signals without clipping or saturating. Overall, the AD8332 is a versatile and reliable amplifier that can be used in a wide range of RF and microwave applications. It is well-suited for use in a variety of systems, including communication systems, radar systems, and instrumentation systems.

3.7 Demodulation

To demodulate our signal using the process described in The AD8333[23] is an integrated circuit (IC) that can be used to demodulate an amplitude-modulated (AM) signal. It contains all the necessary circuitry to detect and extract the information contained in an AM signal. In AM, the information is encoded in the amplitude of the carrier wave, which is modulated or varied in some way to convey the information. The AD8333 is able to detect these variations in the carrier wave and extract the original information from the signal. To do this, the AD8333 uses a process called envelope detection. It rectifies the input signal, which removes the negative portions of the waveform, and then filters the resulting signal to remove any remaining high-frequency components. This leaves only the envelope of the original modulated signal, which contains the encoded information. The AD8333 also includes amplifier and buffer stages to amplify the detected envelope and prepare it for further processing or application. It is often used in radio communication systems, industrial control systems, and other applications where an AM signal needs to be demodulated and the information contained in the signal needs to be extracted.

3.8 Sample/Hold

3.9 Pulse-Repetition and Wall Filter

3.10 Amplifier

3.11 Mixer

3.12 Adder

Bibliography

[1] S. Satomura, T. Yoshida, M. Mori, Y. Nimura, G.-i. Hikita, S. Takagishi, and K. Nakanishi, "Analysis of heart motion with ultrasonic Doppler method and its clinical application," *American Heart Journal*, vol. 61, pp. 61–75, 1 January 1961, ISSN: 00028703. DOI: 10.1016/0002-8703(61)90517-8. [Online]. Available: https://linkinghub.elsevier.com/retrieve/pii/0002870361905178.

[2] D. Baker, "Pulsed Ultrasonic Doppler Blood-Flow Sensing," *IEEE Transactions on Sonics and Ultrasonics*, vol. 17, pp. 170–184, 3 Jul. 1970, ISSN: 0018-9537. DOI: 10.1109/t-su.1970.29558. [Online]. Available: http://ieeexplore.ieee.org/document/1538563/.

[3] K. K. Shung and G. A. Thieme, *Ultrasonic scattering in biological tissues*. CRC Press, 1993, p. 499, ISBN: 9780849365683. [Online]. Available: https://www.routledge.com/Ultrasonic-Scattering-in-Biological-Tissues/Shung-Thieme/p/book/9780849365683.

[4] J. A. Jensen, "An Analysis of Pulsed Wave Ultrasound Systems for Blood Velocity Estimation," *Acoustical Imaging*, L. T. Piero and Masotti, Eds., pp. 377–384, 1996. DOI: 10.1007/978-1-4419-8772-3_61. [Online]. Available: http://link.springer.com/10.1007/978-1-4419-8772-3%5C%5F61.

[5] P. J. Fish, "Ultrasonic investigation of blood flow," *Proceedings of the Institution of Mechanical Engineers, Part H: Journal of Engineering in Medicine*, vol. 213, pp. 169–180, 3 March 1999, Pmid: 10420772. DOI: 10.1243/0954411991534898. [Online]. Available: https://doi.org/10.1243/0954411991534898.

[6] T. Jansson, H. W. Peresson, and K. Lindström, "Estimation of blood perfusion using ultrasound," *Proceedings of the Institution of Mechanical Engineers, Part H: Journal of Engineering in Medicine*, vol. 213, pp. 193–193, 3 March 1999, ISSN: 0954-4119. DOI: 10.1243/0954411991534915. [Online]. Available: http://journals.sagepub.com/doi/10.1243/0954411991534915.

[7] P. Munk, "Estimation of blood velocity vectors using ultrasound," Technical University of Denmark, 2000. [Online]. Available: https://findit.dtu.dk/en/catalog/537f0d537401dbcc1200be04.

[8] E. Picano, "Sustainability of medical imaging," *Bmj*, vol. 328, pp. 578–580, 7439 March 2004, ISSN: 0959-8138. DOI: 10.1136/bmj.328.7439.578. [Online]. Available: https://www.bmj.com/lookup/doi/10.1136/bmj.328.7439.578.

[9] E. Chérin, R. Williams, A. Needles, G. Liu, C. White, A. S. Brown, Y.-Q. Zhou, and F. S. Foster, "Ultrahigh frame rate retrospective ultrasound microimaging and blood flow visualization in mice in vivo," *Ultrasound in Medicine & Biology*, vol. 32, pp. 683–691, 5 May 2006, ISSN: 03015629. DOI: 10.1016/j.ultrasmedbio.2005.12.015. [Online]. Available: https://linkinghub.elsevier.com/retrieve/pii/S0301562906000172.

[10] *EL7104 High Speed, Single Channel, Power MOSFET Driver*, Renesas Electronics, Jun. 2006. [Online]. Available: https://www.renesas.com/us/en/document/dst/el7104-datasheet.

[11] X. Xu, J. Yen, and K. K. Shung, "A low-cost bipolar pulse generator for high-frequency ultrasound applications," *IEEE Transactions on Ultrasonics, Ferroelectrics and Frequency Control*, vol. 54, pp. 443–447, 2 February 2007, ISSN: 0885-3010. DOI: 10.1109/tuffc.2007.259. [Online]. Available: http://ieeexplore.ieee.org/document/4107704/.

[12] *OPA847 Wideband VF Operational Amplifier*, Texas Instruments, Inc., 2008. [Online]. Available: https://www.ti.com/lit/ds/symlink/opa847.pdf.

[13] I. K. H. Tsang, B. Y. S. Yiu, D. K. H. Cheung, H. C. T. Chiu, C. C. P. Cheung, and A. C. H. Yu, "Design of a multi-channel pre-beamform data acquisition system for an ultrasound research scanner," Ieee, Sep. 2009, pp. 1840–1843, ISBN: 978-1-4244-4389-5. DOI: 10.1109/ultsym.2009.5441869. [Online]. Available: http://ieeexplore.ieee.org/document/5441869/.

[14] E. A. Aydn and . Güler, "Design Of Pic-controlled Pulsed Ultrasonic Transmitter For Measuring Gingiva Thickness," *Instrumentation Science & Technology*, vol. 38, pp. 411–420, 6 October 2010, ISSN: 1073-9149. DOI: 10.1080/10739149.2010.509149. [Online]. Available: http://www.tandfonline.com/doi/abs/10.1080/10739149.2010.509149.

[15] N. Matsuoka, D.-G. Paeng, R. Chen, H. Ameri, W. Abdallah, Q. Zhou, A. Fawzi, K. K. Shung, and M. Humayun, "Ultrasonic Doppler measurements of blood flow velocity of rabbit retinal vessels using a 45-MHz needle transducer," *Graefe's Archive for Clinical and Experimental Ophthalmology*, vol. 248, pp. 675–680, 5 2010, ISSN: 1435-702x. DOI: 10.1007/s00417-009-1298-9. [Online]. Available: https://doi.org/10.1007/s00417-009-1298-9.

[16] K. L. Hansen, M. B. Nielsen, and J. A. Jensen, "In-vivo studies of new vector velocity and adaptive spectral estimators in medical ultrasound," 2011. [Online]. Available: https://orbit.dtu.dk/en/publications/in-vivo-studies-of-new-vector-velocity-and-adaptive-spectral-esti.

[17] C.-C. Huang, P.-Y. Lee, P.-Y. Chen, and T.-Y. Liu, "Design and implementation of a smartphone-based portable ultrasound pulsed-wave doppler device for blood flow measurement," *IEEE Transactions on Ultrasonics, Ferroelectrics and Frequency Control*, vol. 59, pp. 182–188, 1 January 2012, ISSN: 0885-3010. DOI: 10.1109/tuffc.2012.2171. [Online]. Available: http://ieeexplore.ieee.org/document/6138742/.

[18] C. A. Winckler, P. R. Smith, D. M. J. Cowell, O. Olagunju, and S. Freear, "The design of a high speed receiver system for an ultrasound array research platform," Ieee, October 2012, pp. 1481–1484, ISBN: 978-1-4673-4562-0. DOI: 10.1109/ultsym.2012.0370. [Online]. Available: http://ieeexplore.ieee.org/document/6562380/.

[19] J. A. Jensen, *Estimation of Blood Velocities Using Ultrasound: A Signal Processing Approach*, Third Edition. Department of Electrical Engineering, Technical University of Denmark, August 2013, ISBN: 9780521464840.

[20] T. L. Szabo, *Diagnostic Ultrasound Imaging: Inside Out*, Second Edition. Elsevier, 2014, ISBN: 9780123964878. DOI: 10.1016/c2011-0-07261-7. [Online]. Available: https://linkinghub.elsevier.com/retrieve/pii/C20110072617.

[21] K. K. Shung, *Diagnostic Ultrasound: Imaging and Blood Flow Measurements*, Second Edition. CRC Press, December 2015, ISBN: 978-1-4665-8264-4.

[22] *AD8332 Ultralow Noise VGAs with Preamplifier and Programmable R_{IN}*, Analog Devices, May 2016. [Online]. Available: https://www.analog.com/media/en/technical-documentation/data-sheets/AD8331_8332_8334.pdf.

[23] *AD8333 DC to 50 MHz, Dual I/Q Demodulator and Phase Shifter*, Analog Devices, May 2016. [Online]. Available: https://www.analog.com/media/en/technical-documentation/data-sheets/AD8333.pdf.

[24] P. Govindan, B. Wang, P. Ravi, and J. Saniie, "Hardware and software architectures for computationally efficient three-dimensional ultrasonic data compression," *IET Circuits, Devices & Systems*, vol. 10, pp. 54–61, 1 January 2016, ISSN: 1751-858x.

DOI: 10.1049/iet-cds.2015.0083. [Online]. Available: https://onlinelibrary.wiley.com/doi/10.1049/iet-cds.2015.0083.

[25] B. Wang and J. Saniie, "Ultrasonic Signal Acquisition and Processing platform based on Zynq SoC," vol. 2016-August, Ieee, May 2016, pp. 0448–0451, ISBN: 978-1-4673-9985-2. DOI: 10.1109/eit.2016.7535282. [Online]. Available: http://ieeexplore.ieee.org/document/7535282/.

[26] *MD1213 High-Speed Dual-MOSFET Driver*, Microchip Technology, Inc., Jun. 2017. [Online]. Available: https://ww1.microchip.com/downloads/en/DeviceDoc/20005713B.pdf.

[27] B. Wang and J. Saniie, "A High Performance Ultrasonic System for Flaw Detection," Ieee, October 2019, pp. 840–843, ISBN: 978-1-7281-4596-9. DOI: 10.1109/ultsym.2019.8926280. [Online]. Available: https://ieeexplore.ieee.org/document/8926280/.

[28] H. Ding, D. Yang, J. Xu, X. Chen, X. Le, Y. Wang, L. Lin, and J. Xie, "Pulsed Wave Doppler Ultrasound Using 3.7 MHz Pmuts Toward Wearable Blood Flow Measurements," Ieee, January 2020, pp. 400–403, ISBN: 978-1-7281-3581-6. DOI: 10.1109/mems46641.2020.9056430. [Online]. Available: https://ieeexplore.ieee.org/document/9056430/.

[29] B. Jana, R. Biswas, P. K. Nath, G. Saha, and S. Banerjee, "Smartphone-Based Point-of-Care System Using Continuous-Wave Portable Doppler," *IEEE Transactions on Instrumentation and Measurement*, vol. 69, pp. 8352–8361, 10 October 2020, ISSN: 0018-9456. DOI: 10.1109/tim.2020.2987654. [Online]. Available: https://ieeexplore.ieee.org/document/9064842/.

[30] H. Ding, D. Yang, M. Qu, *et al.*, "A Pulsed Wave Doppler Ultrasound Blood Flowmeter by PMUTs," *Journal of Microelectromechanical Systems*, vol. 30, pp. 680–682, 5 October 2021, ISSN: 1941-0158. DOI: 10.1109/jmems.2021.3103756. [Online]. Available: https://ieeexplore.ieee.org/abstract/document/9515180.

[31] *ISL55111 Dual, High Speed MOSFET Driver*, Renesas Electronics, April 2021. [Online]. Available: https://www.renesas.com/us/en/document/dst/isl55110-isl55111-datasheet.

[32] M. Winder, A. J. Owczarek, J. Chudek, J. Pilch-Kowalczyk, and J. Baron, "Are We Overdoing It? Changes in Diagnostic Imaging Workload during the Years 20102020 including the Impact of the SARS-CoV-2 Pandemic," *Healthcare*, vol. 9, p. 1557, 11 November 2021, ISSN: 2227-9032. DOI: 10.3390/healthcare9111557. [Online]. Available: https://www.mdpi.com/2227-9032/9/11/1557.